The Dynamics and Acoustics of Travelling Bubble Cavitation

S. Ceccio, C. Brennen (California Institute of Technology, USA)

ABSTRACT

Individual travelling cavitation bubbles generated on two axisymmetric headforms were detected using a surface electrode probe. The growth and collapse of the bubbles were studied photographically, and these observations are related to the pressure fields and viscous flow patterns associated with each headform. Measurements of the acoustic impulse generated by the bubble collapse are analyzed and found to correlate with the maximum volume of the bubble for each headform. These results are compared to the observed bubble dynamics and numerical solutions of the Rayleigh- Plesset equation. Finally, the cavitation nuclei flux was measured and predicted cavitation event rates and bubble maximum size distributions are compared with the measurements of these quantities.

1. INTRODUCTION

Though the dynamics and acoustics of travelling bubble cavitation have been extensively studied both experimentally and theoretically, the behavior of naturally occurring cavitation bubbles near surfaces has not been examined in great detail. It has been known for some time that cavitation bubbles generated near surfaces are usually not spherical (as often assumed in theory) but hemispherical caps (Knapp and Hollander (1948) and Parkin (1952)), and a cavitation bubble collapsing near a solid boundary may produce a microjet of fluid which has been speculated to cause surface cavitation damage (Benjamin and Ellis (1966), Plesset and Chapman (1970), Lauterborn and Bolle (1975), Kimoto (1987) and, for a review, Blake and Gibson (1987)). The complex shapes that travelling bubbles assume will clearly be influenced by macroscopic flow phenomena such as pressure gradients, boundary layers, separation, and turbulence. Researchers have attempted to study these effects by observing cavitation bubbles induced in a venturi (Kling and Hammitt (1972)) or above a surface (Chahine et. al. (1979), van der Meulen (1989)). Yet detailed, systematic studies of hydrodynamically-produced cavitation bubbles are almost non-existent. The random nature of naturally occurring cavitation is the primary reason why investigators have focused on integral measurements in their study of cavitating flows, leaving the detailed behavior of individual cavitation bubbles unexamined.

Analyses of cavitation noise have generally been based on the theoretical behavior of single, spherical bubbles following the work of Fitzpatrick and Strasberg (1956). From this data base, researchers have synthesized the acoustic emission from cavitating flows with multiple events (Blake (1986)). Many experiments have attempted to extract the actual behavior of individual bubbles from the integral measurement of the noise produced by cavitation (Mellon (1956), Blake, Wolpert, and Geib (1977), Hamilton (1981), Hamilton, Thompson, and Billet (1982), and Marboe, Billet, and Thompson (1986)). Although trends are seen in the measured spectra which may be related to theoretical predictions, the difficulty of obtaining free field acoustic spectra in the confines of most water tunnels has always made interpretation of experimental spectra problematic.

Researchers have also attempted to treat cavitation as a stochastic process. The spectral emission of a cavitating flow will depend not only on the noise produced by single bubbles but also on the cavitation rate and event statistics (Morozov (1969) and Baiter (1986)). Furthermore, cavitation noise scaling like that suggested by Blake, Wolpert, and Geib (1977) will be significantly influenced by changes in the cavitation event rate. As the number of cavitation events increase, bubble interactions will affect individual bubble volume histories and their acoustic emission (e.g. Morch (1982), Arakeri and Shanmuganathan (1985), and d'Agostino, Brennen, and Acosta (1988)). Analyses of multiple bubble effects depend upon a knowledge of the nuclei distribution in the flow and the dynamics causing the nuclei to cavitate.

Yet, the effect of nuclei number distribution on the total cavitation process is poorly understood, and this is due largely to the difficulty of accurately measuring this quantity. In fact, most cavitation studies neglect to include any measure of the nuclei number distribution. As we shall demonstrate, the number and size distribution of cavitation bubbles, and the resulting noise emission, can vary substantially over the course of an experiment, even at a nominally fixed operating point. Although the mean cavitation event rate may be approximately determined by the acoustic pulse rate (Marboe, Billet, and Thompson (1986)), cavitation bubble size distributions have only been determined in very rough form (Baiter (1974) and Meyer, Billet, and Holl (1989)). Although knowledge of the cavitation rate and bubble size distribution is essential, no simple method has been found to count and measure cavitation bubbles.

The above observations indicate a need to study the dynamics and acoustic emission of individual cavitation bubbles. A method of detecting and measuring cavitation bubbles was needed, and this paper presents data obtained through the use of a new electrical probe developed for this purpose. Using this new instrument experiments were performed to study individual cavitation events and their statistics in an attempt to address the above issues.

2. NOMENCLATURE

$A(R_O)$	streamtube capture area for given nuclei
C_P	pressure coefficient, $(P - P_0)\,/\,(\frac{1}{2}\rho U^2)$
C_{PM}	minimum pressure coefficient on body surface
f	frequency
I	measured acoustic impulse
I^*	dimensionless acoustic impulse
$N(R_O)$	free stream nuclei distribution
$Pr_O(R_M)$	max. bubble volume distribution associated with nuclei of size R_O
$Pr(R_M)$	maximum bubble volume distribution
P_A	acoustic pressure
P_O	freestream pressure
P_V	water vapor pressure
r	acoustic path length
$R(t)$	calculated bubble radius
R_C	critical nuclei radius
R_B	headform radius at C_{PM}
R_H	headform radius
R_L	bubble radius along trajectory
R_M	cavitation bubble maximum radius
R_{MR}	cavitation bubble maximum reduced radius
R_O	nuclei radius
Re	Reynolds number, UD/ν
S	water surface tension
S_P	acoustic pressure spectral coefficients
t	time
t_1, t_2	integration limits for experimental impulse
T	acoustic pulse duration
T^*	calculated dimensionless pulse duration
U	free stream velocity
$V(t)$	calculated bubble volume
We	Weber number, $\rho U^2 R_H/S$
α	constant, pulse width relationship
β	constant, nuclei stability relationship
κ	headform radius of curvature at C_{PM}
ν	water viscosity
ρ	water density
σ	cavitation number, $(P - P_V)\,/\,(\frac{1}{2}\rho U^2)$
σ_i	bubble cavitation inception index
σ_{ac}	attached cavity formation index
Θ	cavitation event rate

3. EXPERIMENTAL SETUP

The experiments were conducted in the Caltech Low Turbulence Water Tunnel (LTWT);a full description of the facility is presented by Gates (1977). For all experiments, the test section free stream velocity was set and the tunnel static pressure lowered until the desired cavitation number was reached. The operating air content was generally between $6-8ppm$, and the tunnel water was well filtered. The free stream nuclei number distribution of the upstream fluid was measured using in-line pulsed holography. A detailed description of the holographic system is presented by Katz (1981).

Two axisymmetric headforms were used in the present experiments. The first was a Schiebe headform with an ultimate diameter of $5.08cm$. (Gates et al (1979)); the second, which has a modified ellipsoidal shape with a diameter of $5.59cm$, is known as the

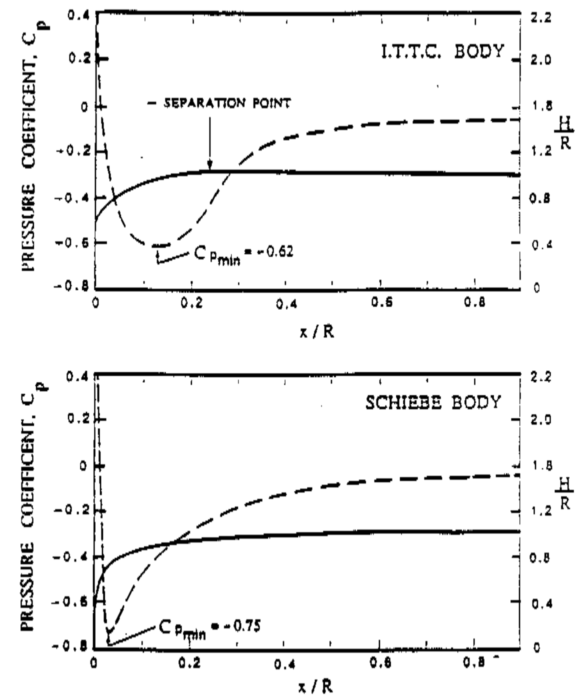

Figure 1. Surface pressure distributions and profiles of the I.T.T.C body and the Schiebe body.

I.T.T.C. headform (Lindgren and Johnsson (1966)). Surface pressure distributions for the Schiebe body (Gates et al (1979)) and the I.T.T.C. headform (Hoyt (1966)) are available in the literature. The headform contours and surface pressure distributions are presented in Figure 1.

The headforms were fabricated out of lucite, a material whose acoustic impedance is a fair match to that of water. The hollow interior of both bodies was filled with water in which a hydrophone was placed. The hydrophone, an ITC-1042, has a relatively flat response out to $80kHz$. Except for ultralow frequencies ($\ll 1Hz$), the hydrophone signal was not filtered. All acoustic signals were digitized at a sampling rate of $1MHz$. Because of the relatively good acoustic impedance match between lucite and water, the interior hydrophone allows the noise generated by the cavitation bubbles to reach the hydrophone relatively undistorted; reflected acoustic signals from other parts of the water tunnel only make their appearance after the important initial signal has been recorded.

In addition to the hydrophone, each headform was provided with novel equipment developed from instrumentation which had previously been used to measure volume fractions in multiphase flows (Bernier (1981)). This instrumentation consisted of a series of electrodes arrayed on the headform surface which were used to detect and measure individual cavitation bubbles. A pattern of alternating electric potentials is applied to the electrodes and the electric current from each is monitored. When a bubble passes over one of the electrodes the impedance of the local conducting medium is altered, causing a change in the current from the electrode. This change, which is detected and recorded, permits the position and volume of the bubble to be monitored.

One specific electrode geometry consisted of patches arrayed in the flow direction to cover the major extent of the cavitating region. Another consisted of electrodes which encircled the entire circumference of the headform in the region of maximum bubble growth. These two electrode geometries were used for different purposes. Signals from the patch electrodes indicated cavitation at a specific location on the headform, and, by electronically triggering flash photography, simultaneous plan and profile photographs of individual bubbles could be taken at a prescribed moment in the bubble history. Thus, a whole series of bubbles could be inspected at the same point in their trajectory. Furthermore, by simultaneously recording the acoustic signal from the hydrophone, one could correlate the noise with the geometry of the bubbles.

The circular geometry was used to detect the occurrence of every cavitation bubble at a particular location on the headform. This position was chosen to be near the location of maximum bubble volume, and for relatively moderate event rates only one bubble would occur over the electrode at any given time. Because almost all the cavitation bubbles maintain the same distance above the electrodes (this will be discussed below), the output of the circular electrode system is directly proportional to the area covered by the bubble, and the peak of the signal is proportional to the major diameter of the bubble base. This system was calibrated photographically and found to be quite linear. The volume of the bubbles was then determined from a measure of the base diameter using a functional relationship derived through the photographic study of many individual bubbles (Ceccio (1990)). Two kinds of experiments were performed with the circular electrode system. The first involved the measurement of event statistics and bubble maximum size distributions. In the second, the acoustic emission of individual cavitation bubbles was analyzed and the result correlated with the bubble maximum volume.

4. OBSERVATIONS OF SINGLE CAVITATION BUBBLES

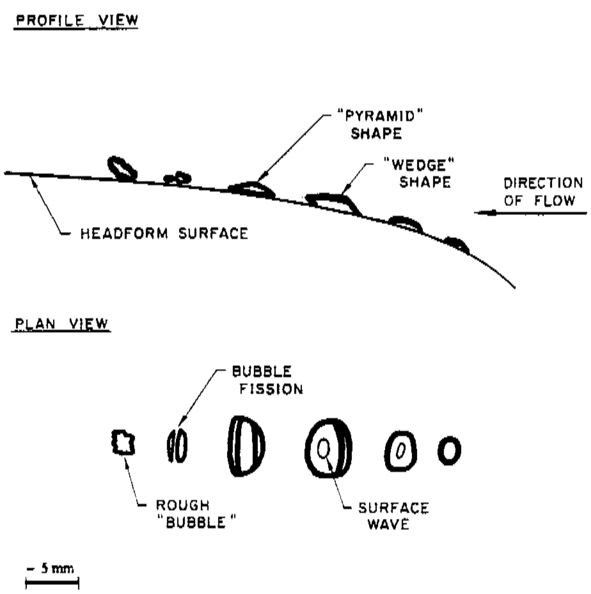

Figure 2. Schematic diagram of typical bubble evolution on the Schiebe headform.

Cavitation bubbles were observed on both the Schiebe and I.T.T.C. headforms over a range of cavitation numbers. The cavitation number was varied between the traveling bubble cavitation inception value, σ_i, and the value at which attached cavitation occurred, $\sigma_a c$. The inception index on both bodies was strongly dependent on the ambient nuclei number distribution (Ooi (1981)). Inception occurred on the Schiebe body at cavitation numbers as high as $\sigma_i = 0.65$, and on the I.T.T.C. body at $\sigma_i = 0.58$ for tunnel water of $6 - 7ppm$ air content. However on both bodies the inception index was reduced to about $\sigma_i = 0.50$ immediately after deaeration. Any definition of the bubble cavitation inception index must therefore be associated with a particular free stream nuclei number distribution. The attached cavitation formation index for the Schiebe body was $\sigma_{ac} = 0.40$ and for the I.T.T.C. body $\sigma_{ac} = 0.41$. These values were almost constant over the fairly narrow range of Reynolds numbers of the experiments ($Re = 4.4\times10^5 - 4.8\times10^5$).

Before detailing the results from each headform, one observation can be made for both geometries. For a given tunnel velocity and cavitation number, the maximum bubble volumes were quite uniform. Although the incoming nuclei diameter ranged over almost three orders of magnitude, the maximum cavitation bubble volume varied over only one order of magnitude. The reason for this is given below.

For both headforms, the growth phase of the nuclei was very similar to that described in the original observations of Knapp and Hollander (1948) and Ellis (1952). For most of their evolution, the bubbles take on a hemispherical or "cap" shape and move extremely close to the headform surface; only very occasionally would quasi-spherical bubbles be observed at a distance above the surface. Small waves could be observed on the bubble surface in many instances. As the bubbles reach their maximum volume they become somewhat elongated in the direction normal to their motion while their thickness normal to the surface remains relatively constant. At this point, the difference in the flows around the two bodies begins to cause differences in the bubble dynamics.

The Schiebe body was designed to suppress laminar separation in the region of cavitation (Schiebe (1972)). It possesses a sharp pressure drop with a minimum pressure coefficient of -0.75 (Figure 1). Figure 2 represents a schematic of the typical bubble evolution, and Figure 3 consists of a series of photographs of bubbles at various stages during this process. After the bubble has reached its maximum volume, it begins to lose its cap-like shape and becomes elongated progressing into a pyramid-like shape; the bubble thickness normal to the headform surface consistently decreases after reaching its maximum. The bubble then collapses rapidly and develops an elongated shape. The elongation of the bubble and the formation of tubes is probably due to rotation of the bubbles caused by the shear in the boundary layer. As the bubble collapses it may fission into two or three tubes of collapsing vapor, and the residual gas in these tubes may cause a rebound to produce a rough bubble or group of bubbles after collapse.

The I.T.T.C. headform has a relatively smooth pressure drop with a minimum pressure coefficient of -0.62. A distinguishing feature of this headform is that, unlike the Schiebe body, it possess a laminar

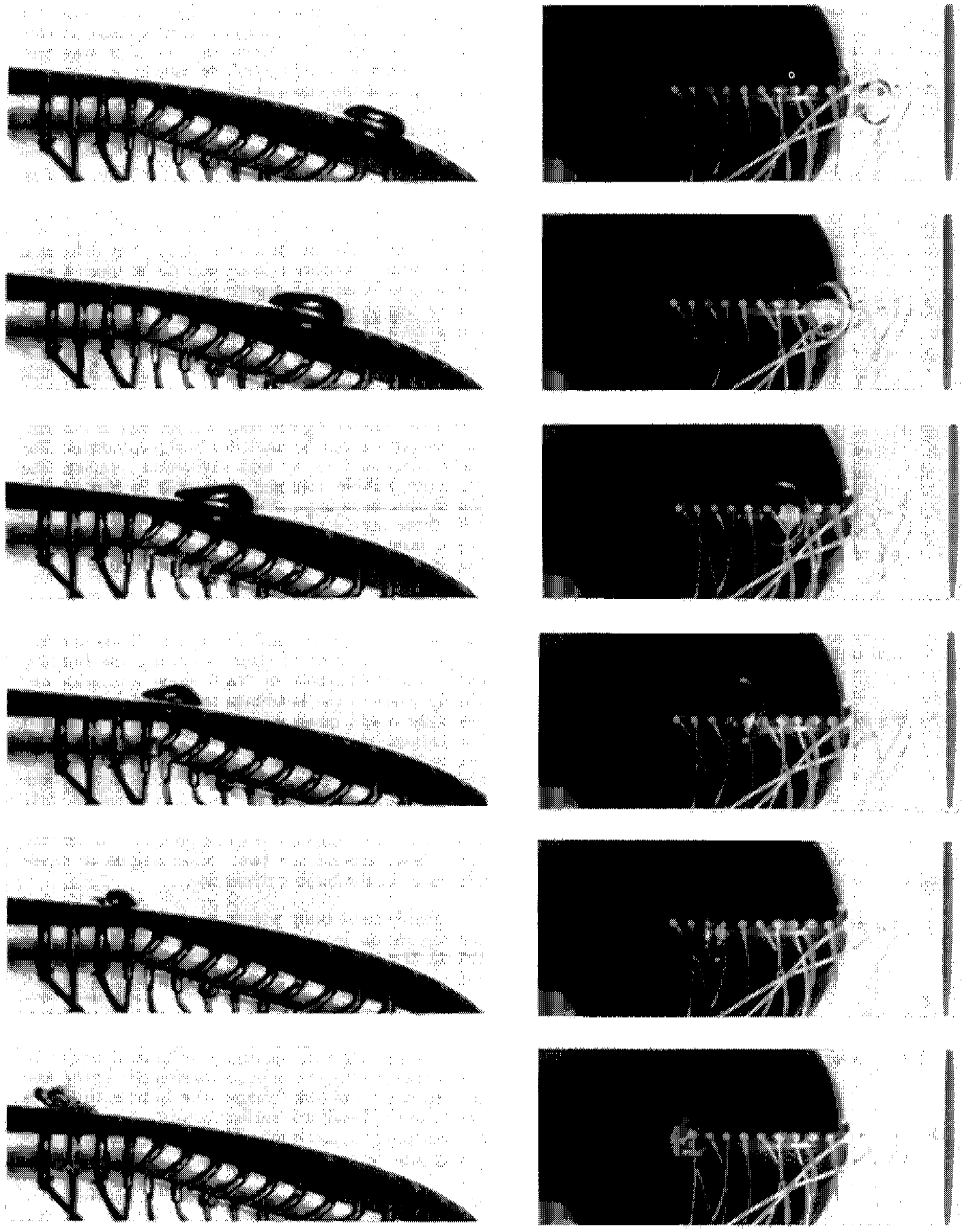

Profile View Plan View

Figure 3. Series of photographs detailing typical bubble evolution on the Schiebe headform, $U = 9m/s$ and $\sigma = 0.45$.

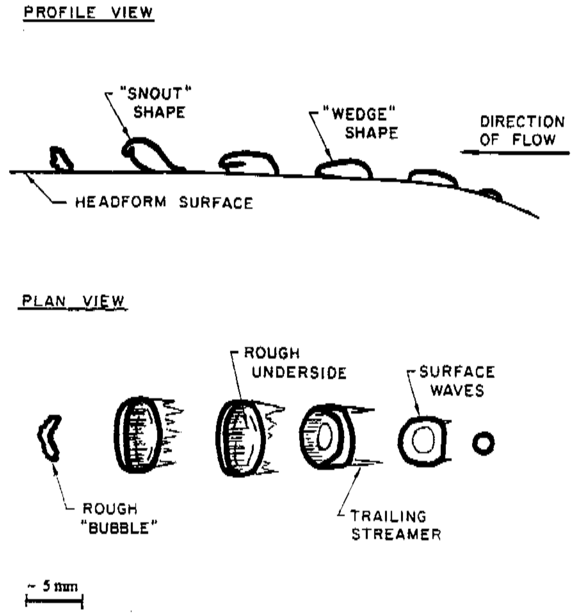

Figure 4. Schematic diagram of typical bubble evolution on the I.T.T.C. headform.

separation region (Figure 1). Figure 4 is a schematic of the typical bubble evolution, and Figure 5 presents a series of photographs of bubbles at various stages of this development. The bubble has a cap-like shape until it reaches its maximum volume where it then becomes further elongated evolving into the wedge-like shape. However, unlike the bubbles on the Schiebe body, the cavity starts to lift off the surface and begins to roll up into a snout-like shape. This may be due to recirculating flow associated with the separation region or the stretching of the bubble in the velocity gradient. As it collapses, the "snout" continues to role up into a vapor tube eventually collapsing to produce a rough bubble after collapse.

On both the Schiebe and I.T.T.C. headforms, the rough bubble or group of bubbles which is formed after collapse is sheared by the surface flow and usually disperses into smaller bubbles on the order of $50\mu m$, although a second collapse and rebound is not uncommon. The mean lifetime of a bubble depends upon the tunnel velocity, cavitation number, and initial nuclei size, but, for most of the observed bubbles on both headforms, it is approximately $3ms$.

The laminar separation on the I.T.T.C. body has been carefully studied in the context of its effect on attached cavitation (Arakeri and Acosta (1973)). Clearly, the separated flow also influences bubble cavitation for cavitation bubbles were observed riding over the separation "bubble". As seen in Figures 4 and 5, the underside of the bubbles become roughened as they pass over the region of turbulent reattachment. These local flow disturbance seem to shear vapor off the underside of the bubble, leaving a trail of much smaller bubbles. This phenomenon was not observed on the Schiebe body.

Furthermore, some bubbles were seen to cause local attached cavitation. When the operating cavitation number was close to the attached cavity formation index, trailing "streamers" were often observed downstream of the cavitation bubble (Figure 6). These streamers were generally associated with the larger bubbles on the I.T.T.C. body (and occasionally on the Schiebe body) and were seen to develop gradually at the location of the laminar separation point (Arakeri and Acosta (1973)). As the bubble is swept downstream, the streamers continue to grow, and in may cases persist even after the bubble has collapsed. Why these bubbles cause the attached cavitation streamers at the lateral extremities of the bubble is unclear. This phenomena has also been observed with travelling bubble cavitation on hydrofoils (van der Meulen (1980), and Rood (1989)). The process could be considered an inception mechanism for attached cavities.

The classic observations of Knapp and Hollander (1949) may be compared those of this study. Both experiments revealed that bubbles travelling near surfaces are cap shaped, and the gross characteristics of growth and collapse are similar. However, the pressure distribution on the ogive of Knapp and Hollander generated a long and steady growth, and the bubbles often retained a quasi-spherical shape even near the final stages of collapse. These bubbles would often rebound many times maintaining their quasi- spherical shape after each collapse. The bubbles observed in this study usually rebounded only once and lost most of their coherent shape after the first collapse. This difference may be explained by noting that the water tunnel facility used by Knapp and Hollander was not equipped with any deaeration system, and extremely bubbly flows were used to increase the odds of photographing a cavitation event. Consequently, the cavitating nuclei observed by Knapp and Hollander were large, containing more undissolved gas. Increasing the amount of residual gas reduces the violence of the bubble collapse making coherent rebounds possible. On the other hand, the nuclei populations of the present study were quite small, and the cavitation bubbles observed were almost entirely vaporous. Such bubbles collapse violently and therefore coherent rebounds are less likely.

Photographs of bubbles presented by Ellis (1952) show many of the features in the present study. Principally, bubbles formed close to the headform also progressed from a cap shape to a wedge shape before collapse, although the collapse mechanism is difficult to distinguish in Ellis' silhouette images. He observed that the bubble surface profile approximately coincided with lines of constant pressure for bubbles near the point of maximum volume. This accounts for the wedge shape of the bubble. Examination of the isobaric lines computed for flow around the Schiebe body (Schiebe (1972)) also show the bubbles observed in this study are being shaped by the pressure gradients close to the surface.

Returning to the present study, the collapse mechanisms for bubbles on both headforms were discerned through the study of many photographs. A composite mechanism is presented in Figure 7 for the Schiebe body with sample photographs in Figure 8. For the I.T.T.C. body similar results are included in Figures 9 and 10. Previous researchers have noted the generation of a liquid microjet in bubbles collapsing near a solid surface (Lauterborn and Bolle (1975) and Kimoto (1987), for example), and this microjet is often identified as the main cause of cavitation erosion damage. Although many photographs were taken during the present investigation, a reentrant microjet was

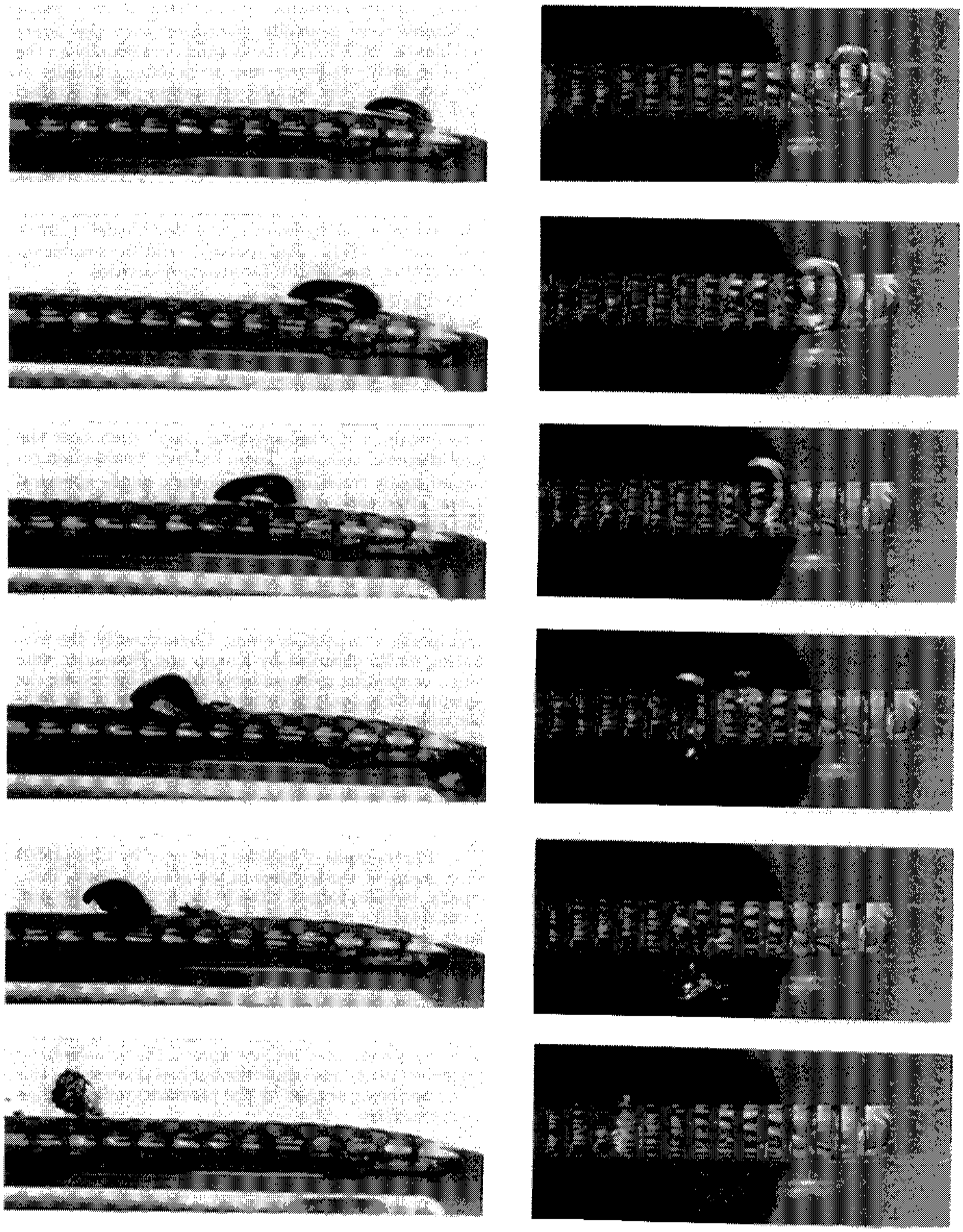

Profile View　　　　　　Plan View

Figure 5. Series of photographs detailing typical bubble evolution on the I.T.T.C. headform, $U = 8.7m/s$ and $\sigma = 0.45$.

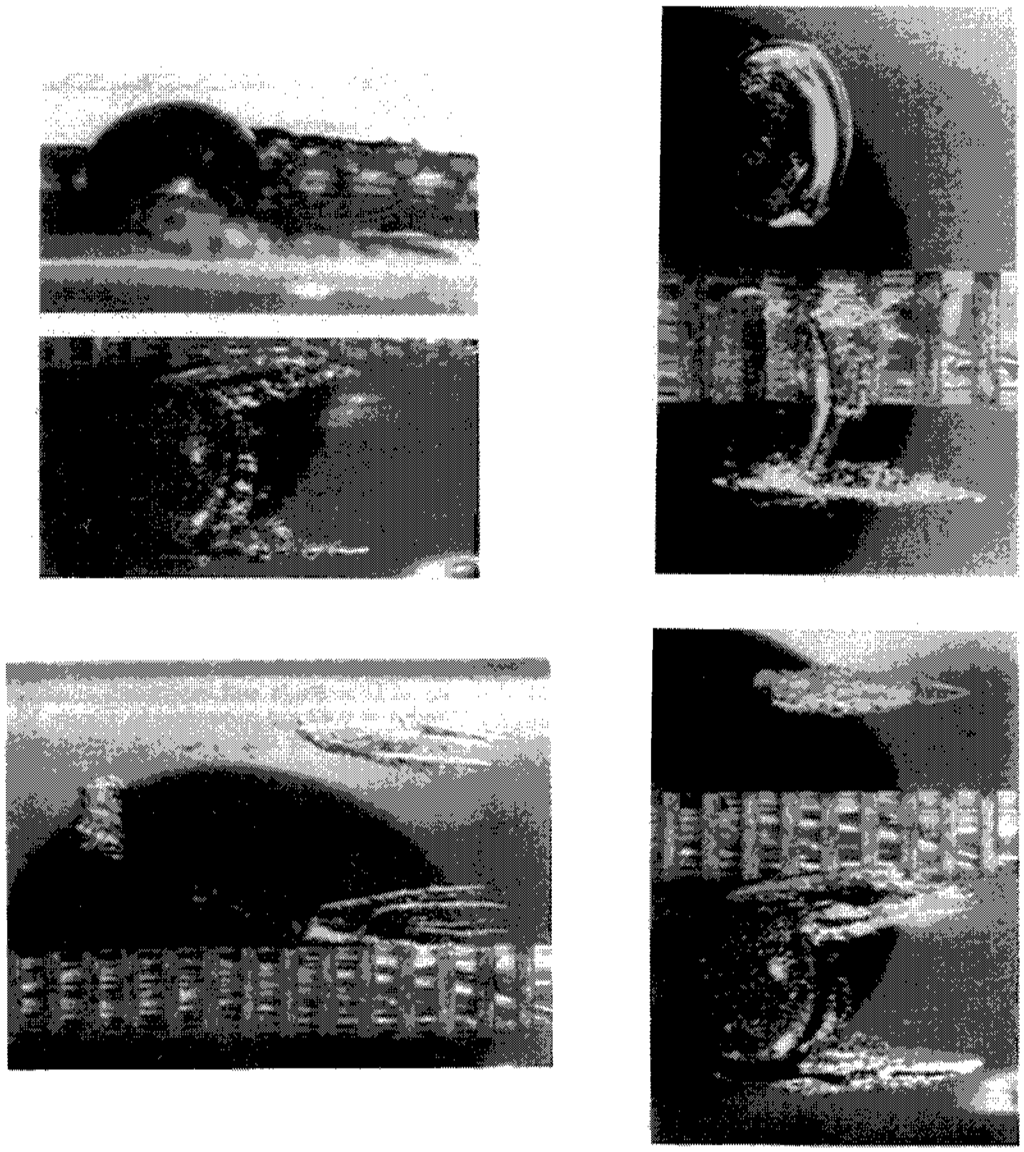

Figure 6. Series of photographs detailing bubbles with tails the I.T.T.C. headform, $U = 9m/s$ and $\sigma = 0.42$.

not observed in any of the present photographs of bubble collapse, although the jet may have occurred too rapidly to be detected. The observed bubbles lack the compact geometry we might expect to be associated with coherent microjet formation.

5. MEASUREMENT OF THE ACOUSTIC EMISSION OF SINGLE CAVITATION BUBBLES

The detailed relationship between the collapse mechanism of hydrodynamic cavitation bubbles and the resulting noise generation is not completely clear, but some features are suggested by the present work. First, as other investigators have concluded (for example Harrison (1952) and Chahine, Courbiere, and Garnaud (1979)), the majority of the noise is generated by the violence of the first collapse; the growth phase contributed no measurable noise signal. The rebound produces a rough bubble which may also collapse to produce a second noise pulse of lesser magnitude. However, noise was not necessarily generated by every bubble collapse. Smaller bubbles would often collapse without an acoustic pulse, and larger bubbles would sometimes produced a muted collapse.

Figure 11 presents two examples of the initial noise pulse generated by the collapse of a bubble on the I.T.T.C. headform. The first pulse has only one peak, but the second trace is an example of a multiple peak event. Multiple peaks suggest bubble fission prior to collapse, and the photographs presented in the previous section reveal that many bubbles have undergone fission.

Although some researchers have used the peak acoustic pressure to characterized cavitation noise intensity (e.g. Van der Meulen (1989)), in this study the magnitude of acoustic pulses will be characterized by the acoustic impulse defined as

$$I = \int_{t_1}^{t_2} P_A dt \tag{1}$$

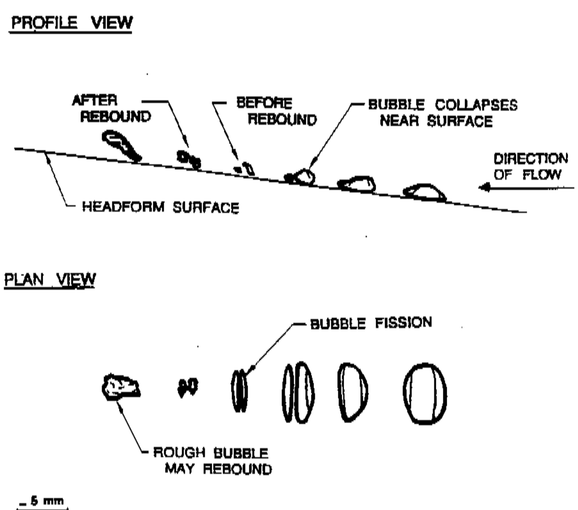

Figure 7. Schematic diagram of typical bubble collapse mechanism on the Schiebe headform.

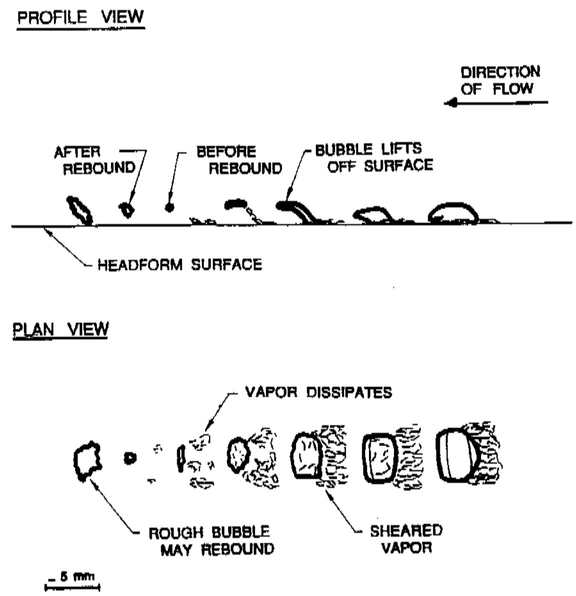

Figure 9. Schematic diagram of typical bubble collapse mechanism on the I.T.T.C. headform.

The times t_1 and t_2 were chosen to exclude the shallow pressure rise before collapse and the reverberation produced after the collapse. Experimentally measured impulses for the Schiebe body at a tunnel velocity of $U = 9m/s$ and cavitation numbers of $\sigma = 0.55$ and $\sigma = 0.42$ are presented in Figure 12 and 13. The data all appear to lie below an envelope which passes through the origin. The existence of this well-defined impulse envelope suggests that a collapsing bubble can generate, for a certain maximum volume, a specific impulse if it collapses in some particular but unknown

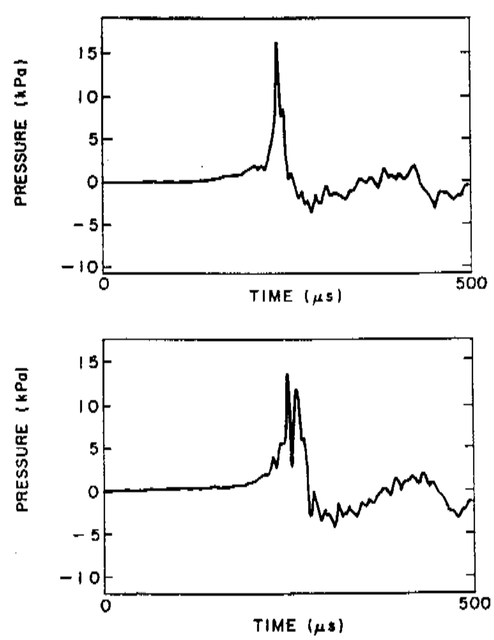

Figure 11. Two examples of typical cavitation initial noise pulses. The bubbles were generated on the I.T.T.C. headform at $\sigma = 0.45$ and $U = 8.7m/s$.

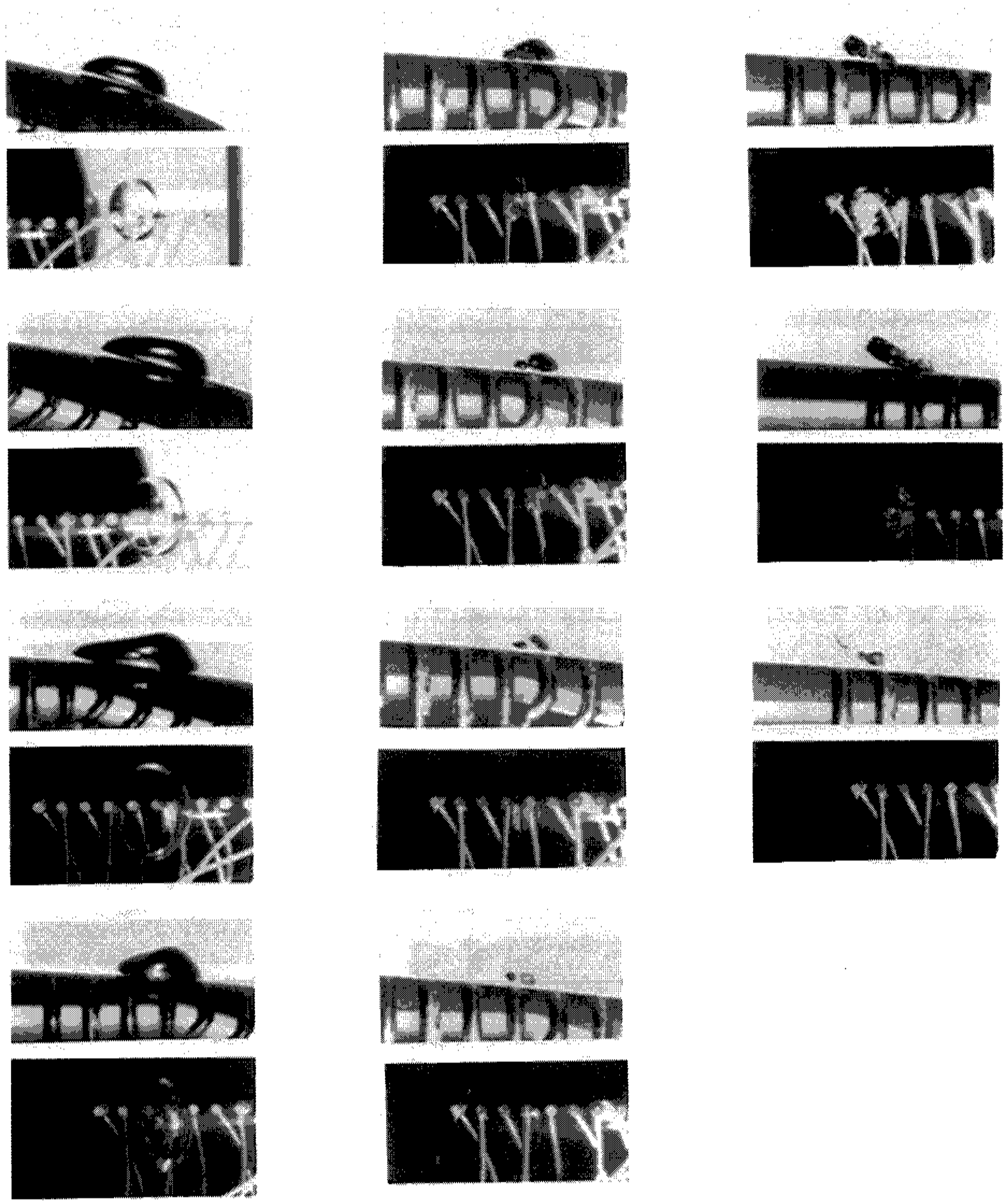

Figure 8. Series of photographs detailing typical bubble collapse mechanism on the Schiebe headform, $U = 9m/s$ and $\sigma = 0.45$.

Figure 10. Series of photographs detailing typical bubble collapse mechanism on the I.T.T.C. headform, $U = 8.7m/s$ and $\sigma = 0.45$.

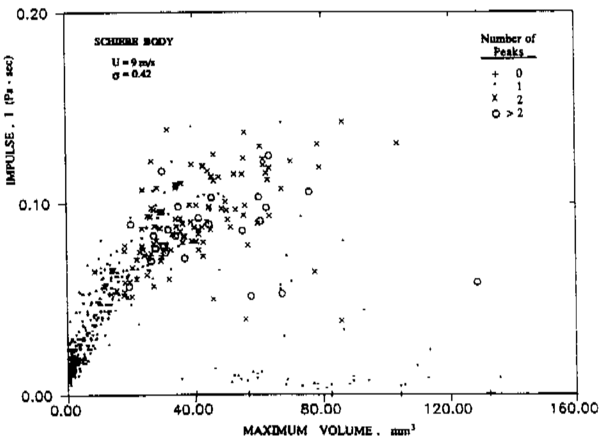

Figure 12. Acoustic impulse plotted against the maximum bubble volume for the Schiebe body at $U = 9m/s$ and $\sigma = 0.42$.

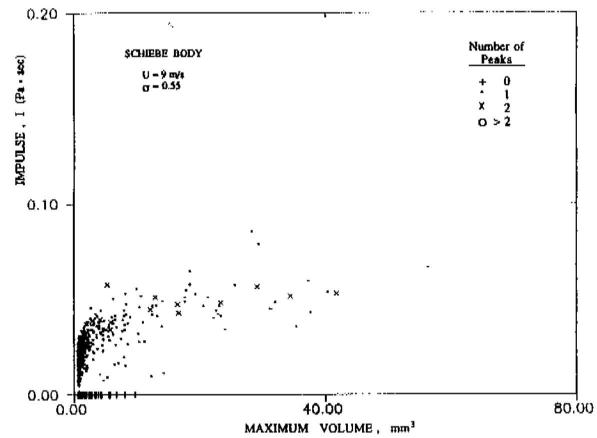

Figure 13. Acoustic impulse plotted against the maximum bubble volume for the Schiebe body at $U = 9m/s$ and $\sigma = 0.55$.

way. It can, however, produce less than this maximum impulse if it collapses in other ways.

The different symbols represent the different number of acoustic peaks which are generated upon collapse. As shown in Figure 12, the probability that a collapse will produce multiple peaks increases for larger bubbles. Yet, even as the number of peaks increases, the impulse often reaches its maximum possible value implying that, in some collapse mechanisms, fission does not decrease the total stored energy available to produce noise. Other large bubbles collapse to produce almost no acoustic impulse. The production of noise upon collapse is the result of violent changes in bubble volume near the point of minimum bubble volume, but larger bubbles may be sheared apart and dissipate thus losing their organized shape and preventing a coherent and concentrated collapse. Furthermore, larger bubbles may contain more contaminant gas (as a result of dissolution) and this would cushion the collapse and reduce the acoustic emission.

At higher cavitation numbers such as that of Figure 13 the number of larger bubbles is reduced, and most bubbles collapse to produce only one acoustic pulse. However, a large number of very small bubbles will collapse and produce no significant impulse, and these cases are represented by the "0" symbols. Mute events are generally not examples of "pseudo-cavitation" as observed by Dreyer (1987) but distinct cavitation events with a near-silent collapse mechanism.

The general trends in the data for the Schiebe body are also evident in the results from the I.T.T.C. headform. Significantly, however, the average acoustic impulse is about three times larger than that of the Schiebe body. This will be discussed further below. Furthermore, as the cavitation number is lowered to near the attached cavitation inception index of the I.T.T.C. body, the impulse data changes significantly. Figure 14 presents an example of data from the I.T.T.C. body taken at a tunnel velocity of $U = 8.7m/s$ and a cavitation number of $\sigma = 0.42$ at near the attached cavitation formation index. The impulses generated by smaller bubbles are much more uncertain, and, for many larger bubbles, no significant impulse is generated. Since these larger bubbles generally have trailing streamers, it would seem that the streamers interfere with the collapse in a way which decreases or eliminates the noise.

The average number of peaks for a given average diameter is plotted in Figure 15 for both headforms. For smaller bubbles, the average is less than unity, reflecting the influence of muted bubbles, and for larger bubbles, multiple peaking produces an average above unity. For the case of the I.T.T.C. body, however, the muting effect of the trailing streamers causes a reduction in the average number of peaks for the data set with the largest average volume. This data set occurs at the lowest cavitation number, near the attached cavitation inception point.

6. COMPARISON WITH ANALYTICAL RESULTS

In order to place the above experimental results in some analytical perspective, calculations were made of the bubble sizes and acoustic impulses predicted by integration of the Rayleigh-Plesset equation starting

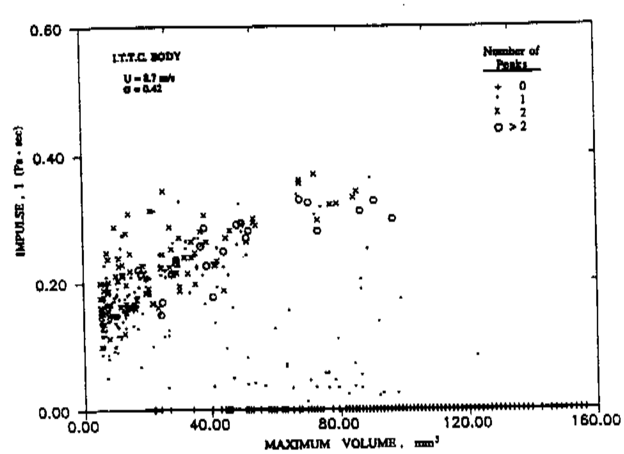

Figure 14. Acoustic impulse plotted against the maximum bubble volume for the I.T.T.C. body at $U = 8.7m/s$ and $\sigma = 0.42$.

with various sizes of freestream nuclei. The known surface pressure distributions for both headforms were employed to construct the pressure-time history which a nucleus would experience while passing near the headform. No slip between the bubble and the liquid and a small offset from the stagnation streamline are assumed. Calculations were performed with various free stream velocities, cavitation numbers, and offsets from the stagnation streamline. Figure 16 provides an example of the dependence of the maximum bubble radius on the original nucleus size for the I.T.T.C. headform and various cavitation numbers. Note that nuclei below a certain size (which depends on the cavitation number) hardly grow at all and would therefore not contribute visible cavitation bubbles. This critical size is predicted by the stability analysis of Johnsson and Hsieh (1966) and Flynn (1964). Bubbles below the critical size grow quasistatically, whereas larger bubbles grow explosively. A bubble is critically unstable if

$$\frac{R_L}{R_H} > \frac{8}{3}\frac{S}{\rho R_H U^2}\frac{1}{(-\sigma - C_{PM})} \tag{2}$$

where C_{PM} is the minimum pressure coefficient (-0.62 for the I.T.T.C. headform) and R_L is the local bubble size. The computations show that so long as the bubble remains stable, then R_L is somewhere in the range $R_O < R_L < 2R_O$ for the common circumstances of interest here. Consequently, the critical nucleus size R_C is given by

$$R_C > \frac{8}{3}\frac{\beta S}{\rho U^2}\frac{1}{(-\sigma - C_{PM})} \tag{3}$$

where β is a constant. The results of this simple expression are presented in Figure 17 along with data on the critical nucleus size obtained from the Rayleigh-Plesset solutions. The qualitative agreement is excellent and suggests a value of β slightly greater that 0.5. Note that the higher the velocity, U, the smaller the critical size, and therefore the larger the number of nuclei that will be involved in cavitation.

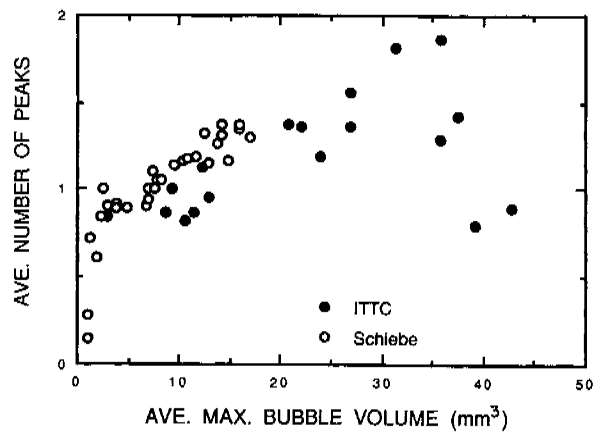

Figure 15. Average number of peaks as a function of average maximum bubble volume for bubbles generated on the Schiebe body and the I.T.T.C. body.

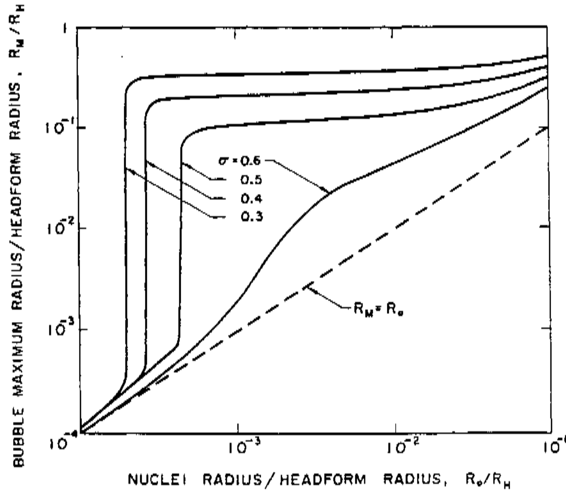

Figure 16. Numerical calculation of the bubble maximum radius as a function of nucleus radius for nuclei passing near the I.T.T.C. headform.

The other feature of Figure 16 which is important to note is that virtually all nuclei greater than the critical nucleus size grow to approximately the same maximum size. The asymptotic growth rate of an unstable cavitating bubble is a function only of the pressure and not the initial nucleus size. Consequently, the maximum size achieved will be approximately independent of the nucleus size. This accounts for the uniformity of cavitation bubbles observed experimentally. Similar calculations were performed for nuclei experiencing the Schiebe body pressure distribution, and the results were qualitatively similar to those of the I.T.T.C. body.

The above calculations yield the volume-time history for a cavitating bubble, and the acoustic pressure generated by the bubble may be approximately given by

$$P_A(r,t) = \frac{\rho}{4\pi r}\frac{d^2V}{dt^2} \tag{4}$$

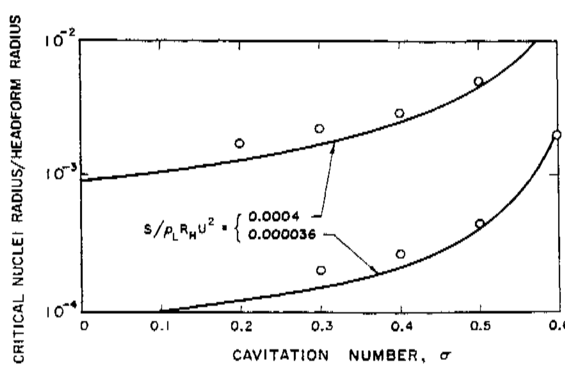

Figure 17. Crital nuclei radius as a function of flow parameters for nuclei passing near the I.T.T.C. headform.

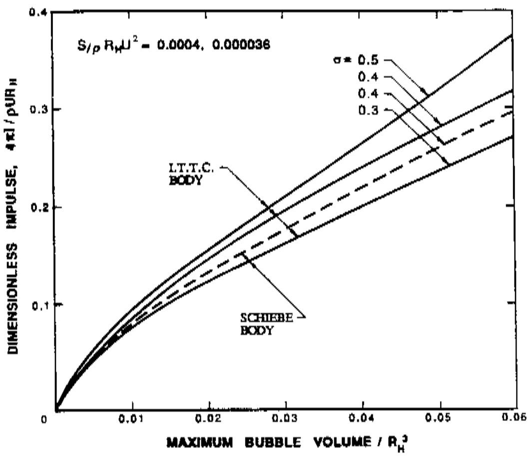

Figure 18. Numerical calculation of the acoustic impulse as a function of the maximum bubble volume for bubbles generated on the Schiebe body and the I.T.T.C. body.

were $V(t)$ is the bubble volume, ρ is the fluid density, and r is the distance from the center of the bubble. This relationship is valid in the acoustic far-field and for subsonic wall velocities. The acoustic impulses, I, were calculated from the definition (1) where t_1 and t_2 were taken to be the times when $d^2V/dt^2 = 0$ before and after the first collapse.

For those nuclei which become unstable and explosively cavitate the non-dimensional impulse, I^*, is defined as

$$I^* = \frac{4\pi I}{\rho R_H U} \tag{5}$$

where we have assumed $r = R_H$ since this is the location of the hydrophone in the experiments. The impulse I^* is plotted in Figure 18 against the maximum volume of the bubbles non-dimensionalized by R_H^3. A number of investigators (i.e. Fitzpatrick and Strasberg (1956) and Hamilton et.al. (1982)) have suggested that the magnitude of the acoustic signal should be related to the maximum size of the bubble, and this is born out in Figure 18 where the data for a range of cavitation numbers and two Weber numbers, We, are contained within a fairly narrow envelope.

The median line was converted to dimensional values and is plotted in Figure 19 where it is compared with data sets from the Schiebe and I.T.T.C. experiments. It is striking to note that the envelope of the maximum impulse from the experiments is within a factor of two of the Rayleigh- Plesset calculation for the I.T.T.C. body and within a factor of six for the Schiebe body. This suggests that, despite the departure from the spherical shape during collapse, the incompressible Rayleigh-Plesset solutions correctly predict the order of magnitude of the noise impulse generated by individual bubbles.

It is not surprising that the predicted impulse is greater than the experimental value. In fact, the theoretical impulse may be considered the maximum impulse possible for a given bubble volume since a spherically symmetric collapse is probably the most efficient noise producing mechanism. The difference between the measured impulses and the theoretical impulse is an indication of the inefficiency of the actual collapse mechanism. Furthermore the average impulses are closer to the theoretically predicted values for the I.T.T.C. body than for Schiebe body, and this is consistent with the photographic evidence that the I.T.T.C. collapse mechanism is more compact than that on the Schiebe body.

The duration of the impulse (as opposed to the magnitude) is much better understood. Here, the duration is defined as $T = t_1 - t_2$. This time is simply related to the total collapse time derived by Rayleigh (1917) which is used by many authors (e.g. Blake, Wolpert, and Geib (1977) and Arakeri and Shanmuganathan (1985)). Like the collapse time, it will be approximated by

$$T^* = \alpha \frac{R_M}{U} \left(\frac{2}{\sigma} \right)^{1/2} \tag{6}$$

where α is some constant of order unity. It follows that the dimensionless impulse duration $T^* = TU/R_H$ should be primarily a function of R_M/R_H, and this is confirmed by the results of the Rayleigh-Plesset solutions shown in Figure 20. Also plotted are typical experimental data from the Schiebe body. Note that the calculated results lie within a narrow envelope for a range of cavitation numbers and that the slope of the narrow envelope is close to unity. The experimental data is about one third the predicted magnitude. Note, however, that the definitions of t_1 and t_2 are somewhat arbitrary.

Figure 21 presents spectra of the noise measured in the experiments. A series of individual acoustic pulses were recorded at a particular velocity and cavitation number. The resulting spectra were averaged to produce the composite spectra in the figure; the

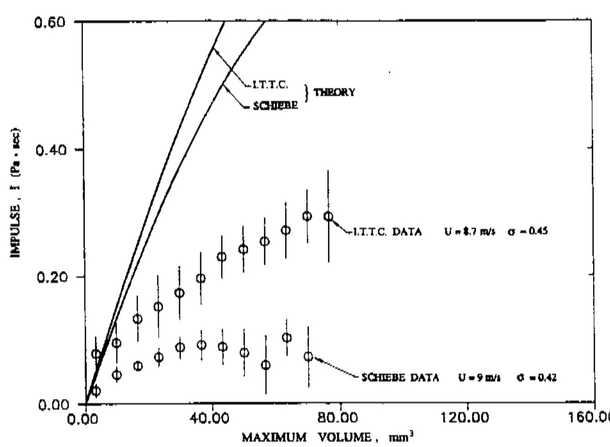

Figure 19. Comparison of theoretically predicted and experimentally measured acoustic impulse as a function of the maximum bubble volume for bubbles generated on the Schiebe body and I.T.T.C. body. Experimental data for $\sigma = 0.45$ and $U = 9m/s$ for the Schiebe body and $U = 8.7m/s$ for the I.T.T.C. body.

signals were not altered to remove the effects of tunnel reverberation. Such a composite spectrum will be equivalent to the spectrum derived from a measurement of a long series of cavitation noise pulses, provided the cavitation events occur randomly (Morozov (1969)). The measured spectral shape varies little with cavitation number; only the overall spectral magnitude changes. A decrease of approximately $-12dB/decade$ is noted until about $100kHz$ where a sharp falloff occurs. This cut-off frequency corresponds to the frequency response limit of the hydrophone.

Asymptotic analyses of the Rayleigh-Plesset equation (Blake (1986)) predict a spectral shape of $f^{-2/5}$ for frequencies in the range of $10kHz$ to $100kHz$. The experimental spectrum has a shape of approximately $f^{-3/5}$ which is similar but not identical to the predicted trend. Hamilton (1981), on the other hand, observed an almost completely flat spectrum in this range based on his integral measurement of bubble cavitation noise. The high frequency roll-off associated with fluid compressibility was not observed below $100kHz$, and this is consistent with the observations of Hamilton (1981) and Barker (1975).

7. OBSERVATIONS OF CAVITATION EVENT RATES AND BUBBLE MAXIMUM SIZE DISTRIBUTIONS

Experiments were performed to measure the cavitation event rate and bubble maximum size distribution on both headforms along with the freestream nuclei number distribution. Furthermore, an analytical model was derived to study the relationship between the nuclei flux and the resulting cavitation statistics.

The cavitation event rate and bubble maximum size distribution were measured for several thousned events at various operating conditions, and examples of these measurements for the Schiebe headform are given in Figure 22. Note that the bubble maximum sizes are presented as reduced radii. The reduced bubble radius is the radius of a sphere of volume equal to the measured bubble volume. Although the four bubble size distributions presented are all at the same cavitation number and tunnel velocity, their event rates and size distributions are quite different. Since the

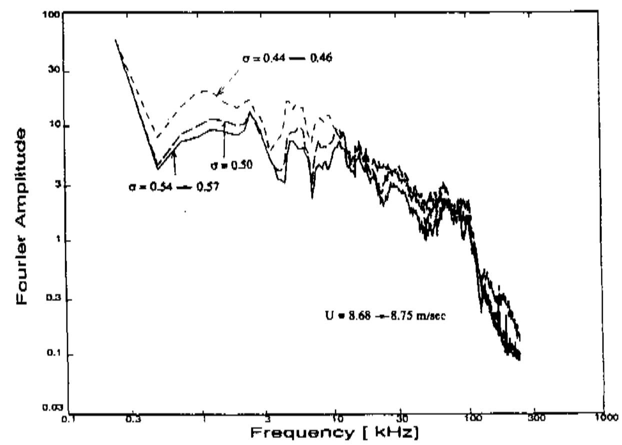

Figure 21. Averaged acoustic spectra derived from acoustic pulses generated by bubbles on the Schiebe body at average $U = 8.7m/s$ and $\sigma = 0.45, 0.50$, and $0.56m/s$.

cavitation bubble maximum volume distribution is directly related to the incoming nuclei number distribution these results clearly indicate that the nuclei number distribution can be quite different for the same tunnel operating conditions. Weak control of the number of nuclei was affected through deaeration and nuclei injection. But, as Figure 22 indicates, the nuclei number distribution is a highly variable factor which influences travelling bubble cavitation and cavitation noise. The time between cavitation events was Poisson distributed, as would be expected for randomly distributed nuclei. Consequently, the total noise spectra produced by these flows should be equivalent to the composite specrtra presented in Figure 21.

A relationship between the nuclei flux and the resulting cavitation event rate and bubble maximum size distribution can be developed as follows. Whether a nucleus cavitates or not is strongly determined by the local minimum pressure it experiences. On the surface of the headform, this pressure is given by the minimum pressure coefficient. On streamlines above

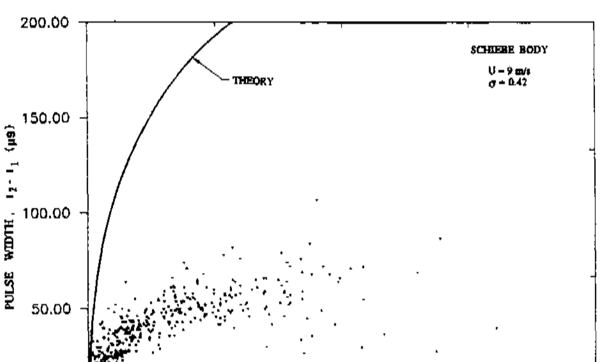

Figure 20. Comparison of theoretically predicted and experimentally measured pulse width as a function of the maximum bubble volume for bubbles on the Schiebe body at $U = 9m/s$ and $\sigma = 0.45$.

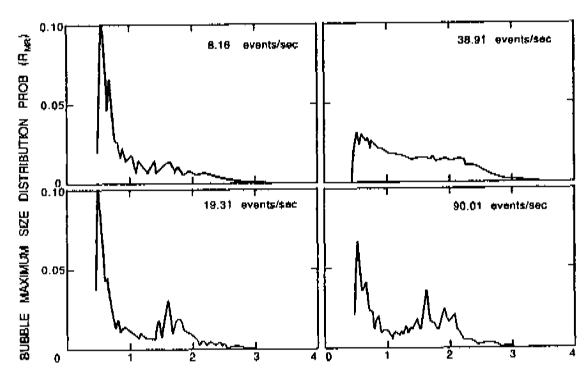

Figure 22. Example of four bubble maximum size distributions for a particular free stream velocity and cavitation number for cavitation on the Schiebe body.

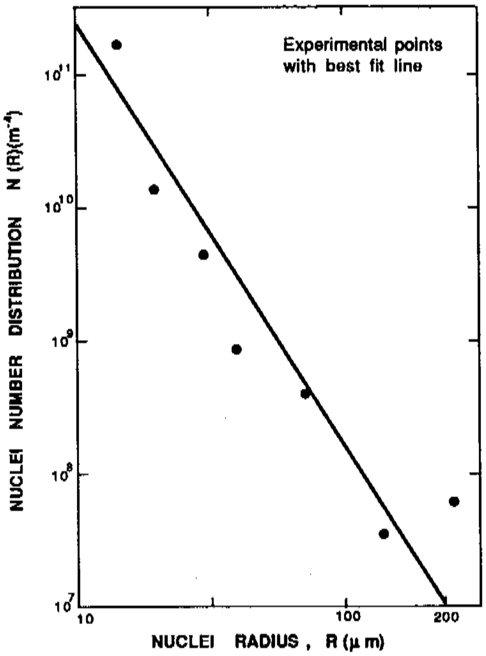

Figure 23. Example measurement of the free stream nuclei number distribution, $U = 9m/s$ and $\sigma = 0.45$.

the body surface, the fluid pressure may still be low enough to cause a nucleus to cavitate provided that the minimum pressure it experiences is below the critical pressure, derived from Equation (3). An incoming streamtube may therefore be defined for a nucleus of specific size such that the nucleus will always encounter a pressure low enough to cause it to cavitate during its flow around the body. The fluid capture area of this streamtube will be a function of the nuclei radius, R_O, the free stream cavitation number, and the flow geometry. By assuming that the pressure gradient normal to the surface corresponds to the centrifugal pressure gradient caused by the radius of curvature, κ, of the surface at the minimum pressure point, and by assuming no slip between the nuclei and the fluid, the following expression for the nuclei capture area, $A(R_O)$, may be readily obtained (Ceccio (1990)):

$$A(R_O) = \frac{R_B \kappa \pi}{\sqrt{1 - C_{PM}}} (-\sigma - C_{PM}) \left(1 - \frac{R_C}{R_O}\right) \quad (7)$$

where R_O is the original nuclei radius, R_B is the headform radius at the point of minimum pressure, and R_C is the minimum cavitatable nucleus given by Equation (3). Equation (7) may be rewritten as

$$A(R_O) = A_V \left(1 - \frac{R_C}{R_O}\right) \quad (8)$$

where A_V is the capture area enclosing all streamlines which involve pressures less than vapor pressure; note that A_V is a function only of the flow geometry and free stream conditions. Finally, the total flux of cavitatable nuclei or total cavitation event rate, Θ, is

$$\Theta = \int_{R_C}^{\infty} A(R_O) N(R_O) U dR_O \quad (9)$$

where $N(R_O)$ is the free stream nuclei number distribution.

Now consider the distribution of bubble maximum sizes which this process will produce. This distribution is the result of different nuclei trajectories and sizes. Cavitating nuclei travelling on streamlines farther away from the headform will not grow to the same maximum volume as those travelling near the surface. Consequently, a flux of uniform nuclei, R_O, will yield a probability distribution distribution of bubble maximum sizes, R_M, denoted by $Pr_O(R_M)$. Because of the slight dependence of bubble maximum size upon nucleus size, Pr_O is a function of R_O. A flux of nuclei represented by the nuclei number distribution, $N(R_O)$, will therefore produce a distribution of maximum bubble sizes, Pr, given by

$$Pr(R_O) = \frac{1}{\Theta} \int_{R_C}^{\infty} Pr_O A(R_O) N(R_O) U dR_O \quad (10)$$

If no relationship existed between nuclei size and the maximum bubble size, Pr would be independent of the nuclei number distribution; changes in $N(R_O)$ would merely change the total event rate. The experimental data indicate, however, that the bubble maximum size distributions are influenced by the nuclei number distribution. The varying event rates reported in Figure 22 indicate different nuclei populations, and each example is accompanied by a unique bubble size distribution. The small influence of nuclei size upon the maximum bubble size will ultimately have a significant influence upon the bubble maximum size distribution.

We shall now compare the measured cavitation event rates and bubble maximum size distributions with the predicted quantities based on holographically-determined free stream nuclei number distributions. The nuclei populations were measured at the same time that the cavitation statistics were recorded, and the smallest nucleus which could be detected with certainty was approximately $20\mu m$ in diameter. An example nuclei distribution is presented in Figure 23. Table 1 presents the measured event rates and the predicted event rates based on Equations (7) and (9). The measured event rates fall within the range of the predicted values, with the uncertainty in the predicted event rates resulting from uncertainty in the measured

PREDICTED Θ (events/sec)	MEASURED Θ (events/sec)
128 $\pm$ 25	156
164 $\pm$ 25	147
147 $\pm$ 25	162

Table 1. Comparison of measured and predicted cavitation event rates for cavitation generated on the I.T.T.C. body at $U = 9m/s$ and $\sigma = 0.45$.

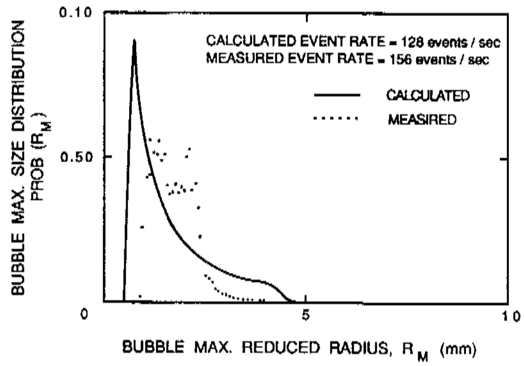

Figure 24. Calculated and measured event rate and bubble maximum size distribution for cavitation on the I.T.T.C. headform at $U = 9m/s$ and $\sigma = 0.45$.

nuclei number distributions. The close match between the predicted and measured event rates indicates that the nucleus stability criteria from Equation (3) adequately models the actual cavitation process. The minimum cavitatable nucleus for this flow is calculated to be approximately $20\mu m$ in radius, and the measured nuclei number distribution indicate that most of the cavitating nuclei are in the range 20 to $100\mu m$. The success of the model suggests that the quantities A_V and R_C may be used to adequately characterize the nuclei capture area for flows over more complicated bodies.

The calculated bubble maximum volume distributions, however, depart substantially from the measured size distribution in terms of its details. Figure 24 presents a measured bubble maximum size distribution along with the predicted distribution based on Equations (7), (9), and (10), the results of Figure 16, and the measured free stream nuclei distribution. The calculated size distribution departs substantially from the measured distribution in its details. The predicted bubble size range is about twice the observed size range, and the number of larger bubbles predicted is much smaller than the observed percentage. These discrepancies may be the result of several phenomena. First, the maximum size achieved by a nucleus subjected to a specific pressure history may not be adequately predicted by the Rayleigh- Plesset equation since bubble growth may be limited by the positive pressure gradients above the headform surface. Once the bubble has grown sufficiently, the mean pressure on the bubble surface will be larger than the surface pressure used in the Rayleigh-Plesset calculation, reducing the driving force for bubble growth. Furthermore, the experimental bubble maximum size distributions often show several maxima which were repeatable for nominally fixed operating conditions. These distributions cannot be simulated with simple, smooth nuclei distributions with several well defined peaks. It seems likely that these maxima are the result of a complicated nuclei number distribution. Such detail could not be ascertained using the current holographic nuclei distribution methodology; its existance was only revealed by the electrode system which permits very large quantities of data on bubble size distributions.

8. CONCLUSION

Although theories of individual bubble cavitation abound, this study demonstrates that a great deal may still be learned through the observation of naturally occurring cavitation bubbles, especially bubbles formed in flows near surfaces. Cavitation bubbles are significantly affected by the viscous flow near surfaces, and this in turn effects their noise production and possibly their damage potential. Yet, numerical integration of the Rayleigh-Plesset provided a reasonable base for comparison with the experimentally measured data. The relationship between the nuclei flux and the resulting cavitation was successfully predicted based upon simple parameters derived from the non-cavitating flow around the body, although estimation of the bubble maximum size distribution was more difficult.

By combining the results of this study, cavitation noise may systematically be synthesized. Analysis of cavitation event statistics and size distributions can relate the freestream nuclei distribution to the cavitation process. And, once the number and size of the cavitation events are known, the total noise emission may be estimated based on the single bubble measurements. The results presented here are useful for the case of limited cavitation, but multiple bubble effects must be included to characterize flows in which the bubbles interact with one another. The importance of the nuclei number distribution as a parameter in cavitation studies cannot be overemphasized, although simple and accurate methods are still needed to measure this quantity with speed, ease, and precision.

ACKNOWLEDGEMENTS

The authors would like to thank Professor Allan Acosta for his advice and considerations. We would also like to acknowledge the assistance of Sanjay Kumar and Douglas Hart. This work was supported by the Office of Naval Research under contract number N-00014-85-K-0397.

REFERENCES

Arakeri, V. H. and Acosta, A. J. 1973. Viscous Effects in the Inception of Cavitation on Axisymmetric Bodies. ASME Journal of Fluids Engineering, Vol. 95, pp. 519-527.

Arakeri, V. H. and Shangumanathan, V. 1985. On the Evidence for the Effect of Bubble Interference on Cavitation Noise. Journal of Fluid Mechanics, Vol. 159, pp. 131-150.

Baiter, H. J. 1974. Aspects of Cavitation Noise. Symposium on High Powered Propulsion of Ships, Wageningen, The Netherlands, Publication No. 490, pp. 1-39.

Baiter, H. J. 1986. On Different Notions of Cavitation Noise and What They Imply. International Symp. on Cavitation and Multiphase Flow Noise, ASME FED Vol. 45, pp. 107-118.

Barker, S. J. 1975. Measurement of Radiated Noise is the Caltech High-Speed Water Tunnel–Part II: Radiated Noise from Cavitating Hydrofoils. Guggenheim Aeronautics Laboratory, California Insitute of Technology Report.

Benjamin, T. B. and Ellis, A. T. 1966. The Collapse of Cavitation Bubbles and the Pressures Thereby Produced Against Solid Boundaries. Philosophical Transactions of the Royal Society of London, Vol. 260, pp. 221-240.

Bernier, J. N. 1981. Unsteady Two-Phase Flow Instrumentation and Measurement. Rep. E200.4, California Institute of Technology, Division of Engineering and Applied Science.

Blake, J. R. and Gibson, D. C. 1987. Cavitation Bubbles Near Boundaries. Ann. Rev. Fluid Mechanics, Vol. 19, pp. 99-123.

Blake, W. K., Wolpert, M. J. and Geib, F. E. 1977. Cavitation Noise and Inception as Influenced by Boundary Layer Development on a Hydrofoil. Journal of Fluid Mechanics, Vol. 80, pp. 617-640.

Blake, W. K. 1986. Mechanics of Flow Induced Sound and Vibration. Volume 1, Chapter 6, Introduction to Bubble Dynamics and Cavitation, Academic Press, pp. 370-425.

Ceccio, S. L. 1990. Observations of the Dynamics and Acoustics of Travelling Bubble Cavitation, Rep. E249.11, California Institute of Technology, Division of Engineering and Applied Science.

Chahine, G. L., Courbiere, P. and Garnaud, P. 1979. Correlation Between Noise and Dynamics of Cavitation Bubbles. Sixth Conference on Fluid Machinery, Budapest, Vol. 1, pp. 200-209.

d'Agostino, L., Brennen, C. E. and Acosta, A. J. 1988. Linearized Dynamics of Two-Dimensional Bubbles and Cavitating Flows Over Slender Surfaces. Journal of Fluid Mechanics, Vol. 199, pp. 155-176.

Dreyer, J. J. 1987. Free Stream Microbubble Effects on Travelling Bubble Cavitation Inception on the Schiebe Headform. ARL/PSU Technical Memorandum 87-205.

Ellis, A. T. 1952. Observations on Cavitation Bubble Collapse. Rep. 21-12, California Institute of Technology, Hydrodynamics Lab.

Fitzpatrick, H. M. and Stasberg, M. 1956. Hydrodynamic Sources of Sound. First Symposium on Naval Hydrodynamics, Washington, D. C., pp. 241-280.

Flynn , H. G. 1964. Physics of Acoustic Cavitation in Liquids. Physical Acoustics, editor W. P. Mason, Academic Press.

Gates, E. M. 1977. The Influence of Freestream Turbulence, Freestream Nuclei Populations, and Drag Reducing Polymer on Cavitation Inception on Two Axisymmetric Bodies. Rep. E182- 2, California Institute of Technology, Division of Engineering and Applied Science.

Gates, E. M., Billet, M. L., Katz, J., Ooi, K. K., Holl, W. and Acosta, A. J. 1979. Cavitation Inception and Nuclei Distribution - Joint ARL-CIT Experiments. Rep. E244-1, California Institute of Technology, Division of Engineering and Applied Science.

Hamilton, M. F. 1981. Travelling Bubble Cavitation and Resulting Noise. Appl. Res. Lab., Penn. State, Tech. Mem. TM 81-76.

Hamilton, M. F., Thompson, D. E. and Billet, M. L. 1982. An Experimental Study of Travelling Bubble Cavitation and Noise. ASME International Symposium on Cavitation Noise, pp. 25-33.

Harrison, M. 1952. An Experimental Study of Single Bubble Cavitation Noise. Journal of the Acoustical Society of America, Vol. 28, pp. 776-782.

Hoyt, J. W. 1966. Wall Effect on I.T.T.C. Standard Head Shape Pressure Distribution. Contribution to 11th International Towing Tank Conference.

Johnsson, V. E. and Hsieh, T. 1966. The Influence of Gas Nuclei on Cavitation Inception. Proc. Sixth Symposium on Naval Hydrodynamics, Washington D. C.

Katz, J. 1981. Cavitation Inception in Separated Flows. Rep. E183-5, California Institute of Technology, Division of Engineering and Applied Science.

Kling, C. L. and Hammitt, F. G. 1972. A Photographic Study of Spark Induced Cavitation Bubble Collapse. A.S.M.E. Journal of Basic Engineering, Vol. 94, pp. 825-833.

Knapp, R. T. and Hollander, A. 1948. Laboratory Investigations of the Mechanisms of Cavitation. Trans. ASME, July 1948, p. 419.

Kimoto, H. 1987. An Experimental Evaluation of the Effects of a Water Microjet and a Shock Wave by a local Pressure Sensor. International Symposium on Cavitation Research Facilities and Techniques, ASME FED Vol. 57, pp. 217-224.

Lauterborn, W. and Bolle, H. 1975. Experimental Investigation of Cavitation-Bubble Collapse in the Neighborhood of a Solid Boundary. Journal of Fluid Mechanics, Vol. 72, pp. 391-399.

Lindgren, H. and Johnsson, C. A. 1966. Cavitation Inception on Headforms: I.T.T.C. Comparative Experiments. Eleventh International Towing Tank Conference Proceedings, Tokyo.

Marboe, M. L., Billet, M. L. and Thompson, D. E. 1986. Some Aspects of Travelling Bubble Cavitation and Noise. International Symp. on Cavitation and Multiphase Flow Noise, ASME FED Vol. 45, pp. 119-126.

Mellon, R. H. 1956. An Experimental Study of the Collapse of a Spherical Cavity in Water. Journal Acoustic Society of America, Vol. 28, pp. 447-454.

Meyer, R. S., Billet, M. L. and Holl, J. W. 1989. Free Stream Nuclei and Cavitation. International Symp. on Cavitation Inception, ASME FED Vol. 89, pp. 55-62.

Morch, K. A. 1982. Energy Consideration on the Collapse of Cavity Clusters. Applied Scientific Research, Vol. 38, p. 313.

Morozov, V. P. 1969. Cavitation Noise as a Train of Sound Pulses Generated at Random Times. Soviet Physics-Acoustics, Vol. 14, pp. 361-365.

Ooi, K. K. 1981. Scale Effects on Cavitation Inception in Submerged Jets. Rep. E183-6, California Institute of Technology, Division of Engineering and Applied Science.

Parkin, B. R. 1952. Scale Effects in Cavitating Flow. Ph.D. Thesis, California Institute of Technology.

Plesset, M. S. and Chapman, R. B. 1970. Collapse of an Initially Spherical Vapor Cavity in the Neighborhood of a Solid Boundary. Rep. 85-49, California Institute of Technology, Division of Engineering and Applied Science.

Rood, E. P. 1989. Mechanisms of Cavitation Inception. International Symp. on Cavitation Inception, ASME FED Vol. 89, pp. 1-22.

Schiebe, F. R. 1972. Measurement of the Cavitation Susceptibility of Water Using Standard Bodies. Rep. No. 118, St. Anthony Falls Hydraulic Laboratory, University of Minnesota.

Van der Meulen, J. H. J. 1980. Boundary Layer and Cavitation Studies of NACA 16-012 and NACA 4412 Hydrofoils. Thirteenth Symposium on Naval Hydrodynamics, Tokyo.

Van der Meulen, J. H. J. and van Renesse, R. L. 1989. The Collapse of Bubbles in a Flow Near a Boundary. Seventeenth Symposium on Naval Hydrodynamics, The Hague.

DISCUSSION

William B. Morgan
David Taylor Research Center, USA

This paper presents a very interesting investigation of cavitation acoustics and the authors are congratulated for such a fine and thorough piece of work. I have one question concerning Fig. 19. This figure shows a significant difference between the acoustic impulses from the "I.T.T.C." headform and the "Schiebe" headform. Do the authors feel this difference is due to the difference in the way the bubbles collapse relative to the headform or do you think there would be an actual difference in the radiated noise?

AUTHORS' REPLY

The authors would like to thank Dr. Morgan for pointing out this phenomena. The significant difference in the average acoustic impulse measured for the two headforms prompted the authors to investigate several factors which could explain the difference. Care was taken to accurately measure the true bubble maximum volume, since bubbles on the I.T.T.C. body were often larger than those on the Schiebe body. Yet, bubbles of equal maximum volume on the two headforms were found to produce significantly different impulses. In fact, a listener standing near the tunnel could easily detect the difference in the acoustic emission between the two headforms. Consequently, the authors have concluded that different acoustic impulses generated by bubbles of equal maximum volume result from the significant difference in the bubble collapse mechanisms, in turn influences the radiated noise.